

OPA-Pack: Object-Property-Aware Robotic Bin Packing

Jia-Hui Pan, Yeok Tatt Cheah, Zhengzhe Liu, Ka-Hei Hui, Xiaojie Gao,
Pheng-Ann Heng, Yun-Hui Liu, and Chi-Wing Fu

Abstract—Robotic bin packing aids in a wide range of real-world scenarios such as e-commerce and warehouses. Yet, existing works focus mainly on considering the shape of objects to optimize packing compactness and neglect object properties such as fragility, edibility, and chemistry that humans typically consider when packing objects. This paper presents OPA-Pack (Object-Property-Aware Packing framework), the first framework that equips the robot with object property considerations in planning the object packing. Technical-wise, we develop a novel object property recognition scheme with retrieval-augmented generation and chain-of-thought reasoning, and build a dataset with object property annotations for 1,032 everyday objects. Also, we formulate OPA-Net, aiming to jointly separate incompatible object pairs and reduce pressure on fragile objects, while compacting the packing. Further, OPA-Net consists of a property embedding layer to encode the property of candidate objects to be packed, together with a fragility heightmap and an avoidance heightmap to keep track of the packed objects. Then, we design a reward function and adopt a deep Q-learning scheme to train OPA-Net. Experimental results manifest that OPA-Pack greatly improves the accuracy of separating incompatible object pairs (from 52% to 95%) and largely reduces pressure on fragile objects (by 29.4%), while maintaining good packing compactness. Besides, we demonstrate the effectiveness of OPA-Pack on a real packing platform, showcasing its practicality in real-world scenarios.

Index Terms—Robotic bin packing, manipulation planning, object property

I. INTRODUCTION

ROBOTIC bin packing has a long history in robotic research. In short, the goal is to deploy the robot arm to automate the packing of objects into a container box. This capability is vital for unmanned intelligent package systems, for example, in e-commerce automation and warehouse logistics. Compared to traditional manual packing, an automated approach helps reduce labor costs, increase overall throughput, and improve workflow stability. For decades, robotic bin packing has been treated mainly as a geometry problem [1]–[11]. The research effort focuses on innovating algorithms to maximize space utilization by considering the shape of

objects in order to pack more objects into the container. Several approaches have been proposed for this goal: (i) optimization-based methods [12]–[18], which identify compact packing solutions through sampling and comparison, (ii) packing heuristics [8], [9], [11]–[13], which propose objective functions to assess packing compactness of different object and placement options, and (iii) reinforcement learning [1], [3], [6], [7], [19]–[23], which develops a packing policy for long-term packing compactness. So far, only a few works [24], [25] study the balance of weights by distributing heavy objects in the container to reduce stress of objects.

In real life, bin packing is not just a geometry problem. When humans pack objects, we consider not only the object geometry but also the object semantics. For example, we try not to damage fragile objects by avoiding to put heavy objects on fragile ones. Similarly, sharp objects are kept away from soft ones such as fruits. Also, considering food contamination, we would separate food from household chemicals. The lack of considering object properties makes existing robotic bin-packing methods less effective for practical usage. Recently, with advances in artificial intelligence, we witness radical changes in how scene and object semantics can be taken into robot manipulation [26]–[32]. To this end, we are motivated to study how robots may take object properties into account when packing objects into the container.

We started this research work by investigating the properties of objects in bin packing. We then found two practical challenges: (i) how to obtain the object properties and (ii) how to effectively incorporate the properties in the bin packing modeling. First, obtaining the physical characteristics of diverse real-world objects often requires extensive human annotations and external knowledge. Fortunately, with the recent development of powerful foundation models [33], [34] trained on a wide variety of reasoning tasks and data, existing vision-language models began to acquire expansive knowledge and sophisticated multi-modal reasoning capabilities, giving them the potential to enhance robotic intelligence [35] and to help robots understand the materials and physical characteristics of varied objects. Second, introducing object properties to packing learning necessitates the design of an objective to balance the compactness with other goals, along with a multi-step planning process to optimize the packing results.

In this work, we present **OPA-Pack**, a novel **Object Property-Aware Packing** framework for everyday objects. To the best of our knowledge, it is the first packing framework that enables the robot to consider not only the object geometry but also the object properties when planning the object packing. In

Jia-Hui Pan, Xiaojie Gao, Ka-Hei Hui, Pheng-Ann Heng, and Chi-Wing Fu are with the Department of Computer Science and Engineering, the Chinese University of Hong Kong (e-mail: {jhpan21, xjgao, khhui, pheng, cwfu}@cse.cuhk.edu.hk); Yeok Tatt Cheah is with the Hong Kong Centre for Logistics Robotics (e-mail: ytcheah@hkclr.hk); Zhengzhe Liu is with the School of Data Science, Lingnan University (e-mail: zhengzheliu@ln.edu.hk); Yun-Hui Liu is with the Department of Mechanical and Automation Engineering, the Chinese University of Hong Kong (e-mail: yhliu@mae.cuhk.edu.hk).

We thank Ziheng Kang for his valuable contributions in scanning and processing real-world objects for use in real-world experiments.

short, we design OPA-Pack with two stages: (i) object property recognition and (ii) packing learning.

In the first stage, we propose to first recognize object properties, including physical attributes, such as softness, sharpness, fragility, and density, and also semantic categories such as edible, household chemicals, medicines, ignition sources, or flammable items. Importantly, we enhance the recognition by adopting the retrieval augmented generation mechanism [36], [37] to find similar examples from a small set of human-annotated objects, such that we can enrich the contextual understanding of the query object. For challenging properties of fragility and density, we adopt a chain-of-thought reasoning scheme [38]–[41] to estimate the object materials first and then leverage the material knowledge to guide property recognition. Next, we further take object-centric properties into account to discover avoidance relations between objects, *i.e.*, object pairs that should not be packed closely, *e.g.*, household chemicals against edible items and sharp objects against soft objects. To facilitate property-aware packing, we prepare the OPA dataset that contains 1,032 everyday objects with property annotations.

In the second stage, we develop **OPA-Net (Object-Property-Aware packing Network)**. Our OPA-Net jointly optimizes for three goals: (i) avoiding closely-packing unsuitable object pairs, (ii) minimizing pressure on fragile objects, and (iii) enhancing the packing compactness. We design our framework with three encoders to first capture the object geometry, object properties, and container condition, as well as locations of the previously-packed objects. We follow [1] to incorporate an order predictor to choose an object out of a candidate set and a placement predictor to decide the object placement pose and location. Besides, we develop a deep Q-learning scheme and a reward function to optimize the three goals simultaneously.

By incorporating object properties into the packing logic, our OPA-Pack is able to produce packing solutions that better protect the packed objects while optimizing the space utilization. Our contributions are summarized as follows:

- We propose OPA-Pack, the first packing framework that equips the robot with object property consideration for more intelligent object packing;
- We design OPA-Net to jointly avoid closely packing unsuitable object pairs and reduce pressure on fragile objects, while optimizing the packing compactness;
- A new property recognition scheme with retrieval-augmented generation and chain-of-thought reasoning is introduced to annotate the object properties;
- We contribute a new dataset of 1,032 objects with property annotations to facilitate property-aware packing which we will release to the public; and
- Experimental results demonstrate that OPA-Pack is able to significantly improve incompatible object pair separation (from 52% to 95%) and greatly reduces pressure on fragile objects (by 29.4%), while maintaining good packing compactness.

II. RELATED WORK

For decades, robotic bin packing has been treated as a geometric problem, in which we aim to maximize the packing

compactness by considering object shapes. This perspective has influenced the development of many algorithms [1], [3], [6]–[9], [11]–[23], which are mainly divided into three categories: optimization-based methods, packing heuristics, and reinforcement learning. However, most of these approaches primarily emphasize geometric modeling, often neglecting the object property such as fragility, edibility, and chemistry.

Optimization-based methods. Several optimization-based approaches have been proposed for robotic bin packing, such as genetic algorithm [12]–[14], tabu search [15], simulated annealing [16], and integer linear programming [17], [18]. Given a set of objects to be packed and an empty container, these methods explore various packing options (including different object orders and varied placement location for each object), comparing multiple solutions to identify a more compact object arrangement. However, they face limitations in robotics due to (i) the need for extensive sampling to plan the entire sequence and (ii) the need to plan again if any object shifts from its intended position during the actual execution. Also, while some works [24], [25] study container balance by distributing heavy objects across various horizontal locations within the container, the aspects of considering object fragility and object avoidance relations remain unexplored.

Packing heuristics. To enable on-the-fly planning in robotic bin packing, several heuristics have been developed [8], [9], [11]–[13]. These heuristics quickly identify the best object choices and placement options in each step of packing an object via specially designed objective functions. For instance, the deepest bottom-left heuristic [13] focuses on deepest, bottom-most, left-most position, the empty-maximal-space [12] suggest placements that maintain a maximal cuboid-shaped empty space, while the heightmap-minimization method [8], [11] suggests placements with minimal heightmap increments, meaning that less space would be wasted under the packed object. Also, the SDF-Minimization method [9] chooses the best-fit object and most compact placement location by minimizing the signed distance field values, achieving highly compact packing. In general, these heuristics are efficient for real-world robotic bin packing. However, they depend on carefully crafted objective functions, so their greedy nature makes it challenging to optimize the final packing results. Further, as far as we know, none of the proposed objectives take object properties into account in the packing process.

Reinforcement learning. On the other hand, RL methods offer a long-horizon optimization and can develop a policy that enhances the overall outcome. Besides, they enable joint optimization of multiple goals through a single reward function, enhancing flexibility and intelligence. Consequently, RL-based packing methods have gained significant attention in recent years [1], [3], [6], [7], [19]–[23]. Initially, [20] designed a classic Deep Q-Network (DQN) that directly takes packing compactness as the reward function to develop an RL-based packing algorithm. Subsequently, various enhancements have been made, including improvements to the network architecture using hierarchical DQN [6] and dueling DQN [1], as well

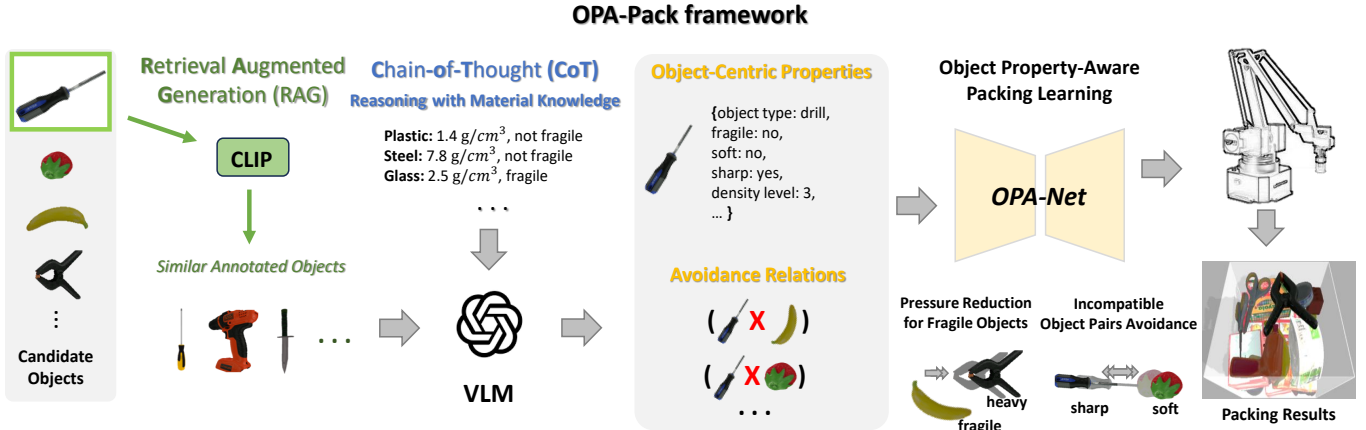


Fig. 1. Illustration of the proposed framework. Our OPA-Pack consists of two stages. In the first stage, we recognize the object properties using a Vision-Language Model (VLM). Retrieval Augmented Generation (RAG) based on CLIP [42] and Chain-of-Thought (CoT) reasoning are used to provide additional information to enhance the recognition. We obtain object-centric properties, *e.g.*, fragility, softness, sharpness, and density levels, and also infer the object relation properties to identify the incompatible object pairs that should not be packed closely with each other. In the second stage, we perform object property-aware packing learning via an OPA-Net to reduce pressure on fragile objects and avoid closely packed incompatible object pairs.

as the integration of object stability [6], [7], [19] and packing heuristics [3] into the reward design. Again, no existing RL-based packing algorithms have considered object properties in their modeling.

Overall, existing methods focus primarily on geometric modeling and typically overlook object properties in the packing planning process. As a result, they could be inadequate in safeguarding fragile items and preventing object contamination for both packing and subsequent storage. This work fills the gap of the existing works, proposing how we can take object properties into account, *e.g.*, to prevent incompatible object pairs and to reduce stress on fragile items. We base our design on reinforcement learning for joint optimization of various objectives and long-horizon planning. To the best of our knowledge, this is the first study to examine object properties in robotic bin packing for everyday objects, aiming for more intelligent robotic packing.

III. OVERVIEW OF OPA-PACK

Robotic bin packing involves multiple steps of packing an object into the container. In each step, given a set of candidate objects and the current container, the packing algorithm selects an object to be packed from multiple candidates and decides its placement location in the container.

To enable such object-property-aware packing, we formulate the OPA-Pack framework into two stages. The framework is illustrated in Figure 1. Procedure-wise, the first stage starts by searching for annotated objects similar to the query object using the CLIP model, then adopting retrieval-augmented generation and chain-of-thought techniques to obtain additional information. This enables us to obtain object-centric properties for each item and subsequently derive relational properties between objects, identifying pairs that should be avoided for close packing. In the second stage, we design the OPA-Net, a specialized neural network built on deep Q-learning, such that we can tailor it to learn property-aware

packing strategies. OPA-Net considers not only the properties of individual extracted objects but also the relational data between objects for selecting the object and computing its placement (orientation and location) in the container in each packing step. It is trained with a novel OPA reward function to jointly separate incompatible pairs and reduce the pressure on fragile objects, while optimizing the overall compactness of the packing.

In the following, we will first introduce the object property recognition scheme in Section IV. Then, we present the object property-aware packing learning scheme in Section V. Finally, we introduce how OPA-Pack performs in test-time in Section VI.

IV. OBJECT PROPERTY RECOGNITION

To perform object-property-aware bin packing, we predict object properties, as illustrated in Figure 2. First, we obtain the object-centric properties via a VLM, with retrieval augmented generation and chain-of-thought reasoning to provide additional examples and physical knowledge to enhance the property recognition. Then the object-centric properties are further employed to identify the property-based avoidance relations, indicating whether pairs of objects should be kept apart during packing. Besides, we construct the OPA dataset, consisting of 1,032 objects with their respective object-centric properties and avoidance relations.

Predicting the Object-centric Properties. First, we predict the object-centric properties, including four physical properties: softness, sharpness, fragility, and density level; and five semantic properties: whether the object is medicine, edible, household chemicals, ignition item, or flammable item. An illustration of the property recognition scheme is shown in Figure 2 (a). This task is challenging, as it requires an understanding of the characteristics of everyday objects. We employ ChatGPT-4 [43] for its strong ability to process language and visual inputs, as well as reason about fundamental concepts.

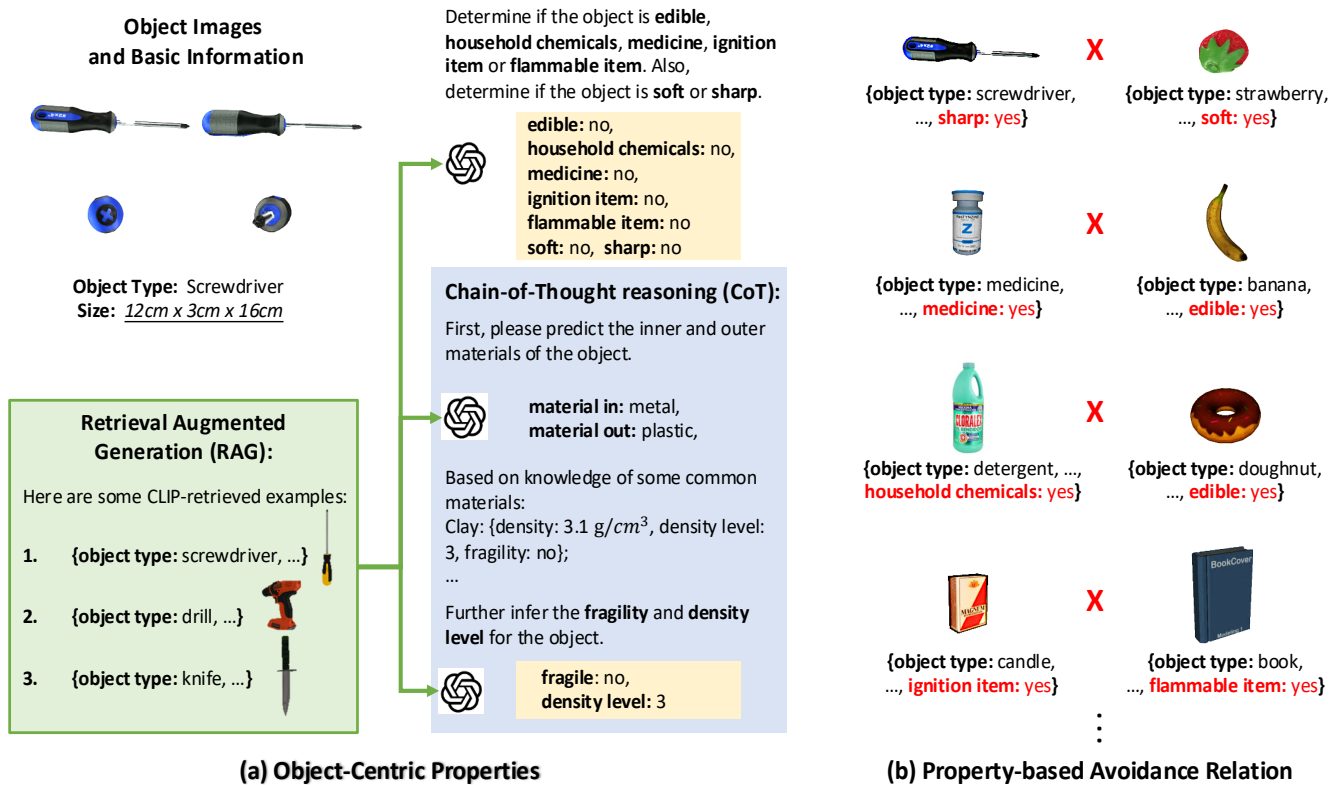


Fig. 2. Our pipeline for object property recognition includes (a) object-centric properties and (b) property-based avoidance relations. For a given object, we provide four views, its class name, and size, and then predict nine object-centric properties (in yellow). To enhance the prediction performance, we provide examples retrieved from a small auxiliary dataset using the CLIP feature, performing RAG (in green). Also, we predict the inner and outer materials of each object and provide additional knowledge of the materials (see Table I), leveraging CoT reasoning to enhance the prediction of fragility and density levels (in blue). Apart from physical properties, we predict also the semantic properties of the object. Besides, we discover the avoidance relations between each pair of objects indicating the object pairs that are not suitable for close packing, considering four types of avoidance relations, i.e., (i) sharp objects v.s. soft objects, (ii) medicine v.s. edible objects, (iii) household chemicals v.s. edible objects, and (iv) ignition items v.s., flammable items. Best viewed in color.

We provide 4 orthogonal views rendered from the 3D model of each object, as well as the size information of the object. Then we perform Retrieval Augmented Generation (RAG) [36], [37] and Chain-of-Thought (CoT) reasoning [38], [39], [41] to enhance the prediction of the object-centric properties.

TABLE I

COMMON MATERIALS WITH DENSITY LEVELS, DENSITY, AND FRAGILITY

Material Name	Density Level	Density (g/cm^3)	Is Fragile?
Air	0	0.0	No
Bread	1	0.3	Yes
Biscuit	1	0.4	Yes
Wood	1	0.4	No
Cardboard	1	0.6	No
Wax	2	0.9	Yes
Water	2	1.0	No
Fruits	2	1.0	Yes
Synthetic (Nylon)	2	1.1	No
Paper	2	1.2	No
Plastic	2	1.4	No
Glass	3	2.5	Yes
Clay	3	3.1	Yes
Ceramic	4	4.2	Yes
Steel	5	7.8	No

To perform RAG, we introduce a small auxiliary database containing 40 example objects from the YCB dataset [44]. Each example object contains manual annotations of its class

name, size, and object-centric properties. For the query object, we retrieve the top-10 most similar example objects from this database using the CLIP [42] visual feature, a multidimensional representation that connects images and text. Specifically, we extract the CLIP features using the front views of the query object and all example objects. Next, we identify the example objects with CLIP features that have the smallest cosine distance to those of the query object. Using the annotations of the retrieved example objects, we guide ChatGPT-4 to predict all five semantic properties and two physical properties, i.e., softness and sharpness.

However, the fragility and the density levels are more challenging to infer from the visual input and a limited number of examples, as these attributes depend on deeper physical knowledge. To tackle this, we adopt CoT reasoning. We first predict the object's inner and outer materials and then provide additional knowledge of fragility and density, as well as how we define the density level to guide the prediction of fragility and density levels. An illustration of the common materials with additional knowledge are provided in Table I. Finally, we ask the ChatGPT-4 to predict the query object's fragility and density levels based on all the previous inputs, the predicted inner and outer materials, as well as the additional knowledge. Please note that the predicted inner and outer materials may not be included in our available knowledge. However, due

the geometries but also the properties of the packed objects and the buffered objects, and decide the packing action a_t based on the updated observation. For (ii), we develop a novel reward function to train the OPA-Net to achieve high packing compactness while reducing pressure on fragile objects and separating the avoidance object pairs.

B. The OPA-Net Architecture

Our OPA-Net enriches the current packing step observation $obs(s_t)$ with object properties and predicts the Q-value for each candidate action a_t . In contrast to previous works [1], [6], [7] that focus on geometry, we incorporate object property encoding and enhance container heightmaps to account for fragile and avoidance objects. The network includes four encoders, *i.e.*, the candidate object’s geometry, candidate poses, object properties, and the container’s heightmaps. It includes two Q-predictors for object and placement decisions, predicting Q-values for each packing action $a_t = \langle b, o, x, y \rangle$, where b is the object, o is the orientation, and x, y are the horizontal placement coordinates. An illustration of the architecture of our network is shown in Figure 4.

Encoding the object geometry. For each candidate object $b \in \mathcal{B}$, we first sample a point cloud \mathbf{P}^b that captures the 3D geometry of the object. Then, we leverage a PointNet [49] $E_P(\cdot)$ as the point cloud feature extractor to encode the geometric feature of the object, as follows:

$$\mathbf{f}_P^b = E_P(\mathbf{P}^b), \quad (4)$$

where \mathbf{f}_P^b denotes the point cloud feature of the object.

Encoding the object candidate poses. For each candidate object, we extract the planner-stable poses [46] to form a set of candidate poses represented in quaternions. We use planner-stable poses because they are the poses that objects are most likely to assume when picked up from the table or conveyor. Then, a Multi-Layer Perceptron (MLP) $E_O(\cdot)$ is used to encode the 6D candidate poses. Suppose for object b , a set of planner-stable poses \mathbf{O}^b are found, the pose feature learning is represented as,

$$\mathbf{f}_O^b = \text{concat}([E_O(o^b), \forall o^b \in \mathbf{O}^b]), \quad (5)$$

where b denotes the index of a candidate object and \mathbf{f}_O^b denotes the pose feature.

Encoding the object properties. For the object properties, we represent the fragility, softness, and sharpness of each object in binary scalars, and we also incorporate the estimated density and the volume of the object in floating numbers. The estimated density of the object is given by the mean density of the materials within each density level. Suppose the density level of a candidate object is l , its estimated density is given by the average density of all materials in the same density level $\frac{1}{|D^l|} \sum_{i, \sigma^i \in D^l} \sigma^i$ (see Table I). The input object properties for object b are concatenated to form a property vector \mathbf{v}^b and are encoded by

$$\mathbf{f}_V^b = E_V(\mathbf{v}^b), \quad (6)$$

where $E_V(\cdot)$ denotes the property-embedding layer, which is a multi-layer perceptron, and \mathbf{f}_V^b denotes the learned features.

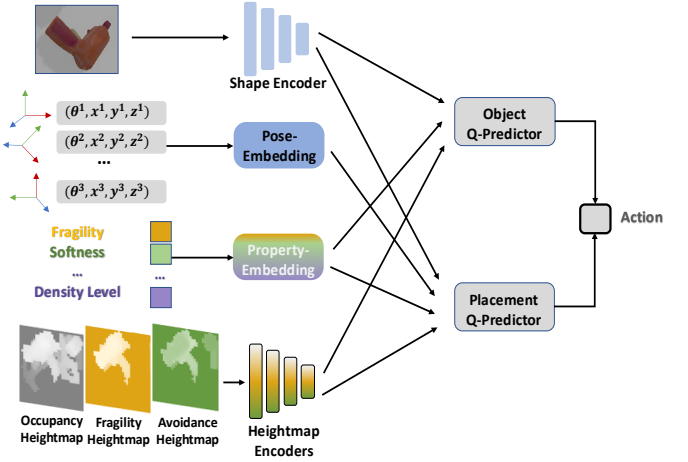


Fig. 4. Illustration of the OPA-Net architecture. The network contains four types of encoders, the shape encoder E_P , the pose-embedding layer E_O , the property-embedding layer E_V , and the heightmap encoders (E_C , E_G and E_D). Then, an object Q-predictor is trained to predict the next object to be packed and a placement Q-predictor is trained to learn the placement of an object. Best viewed in color.

Encoding the container heightmaps. For each candidate object b , our network takes three heightmaps of the container as input, *i.e.*, an occupancy heightmap \mathbf{H}_C , a fragility heightmap \mathbf{H}_G , and an avoidance heightmap \mathbf{H}_D , as shown in the bottom-left part of Figure 4.

\mathbf{H}_C is captured by a depth camera on top of the container, providing a compact representation of the container’s fill level at each location. Additionally, we create a fragility heightmap \mathbf{H}_G to indicate the locations of previously-packed fragile objects by initializing a zeroed 2D map and updating it with the maximum height of each fragile object. The avoidance heightmap \mathbf{H}_D is rendered similarly, only that it uses the avoidance objects towards each candidate object instead of the fragile objects.

Different candidate objects share the same \mathbf{H}_C and \mathbf{H}_G but have distinct \mathbf{H}_D since they could have different avoidance object pairs. For clarity, we denote the avoidance heightmap as \mathbf{H}_D^b for each candidate object b . Unlike \mathbf{H}_C obtained directly from a depth map, \mathbf{H}_G and \mathbf{H}_D^b require the locations of previously-packed fragile and avoidance objects. Therefore, we record all packed objects and their placement locations.

Light-weight Convolutional Neural Networks (CNNs) are leveraged to encode each heightmap, respectively, which is written as follows,

$$\mathbf{f}_C = E_C(\mathbf{H}_C), \quad \mathbf{f}_G = E_G(\mathbf{H}_G), \quad \mathbf{f}_D^b = E_D(\mathbf{H}_D^b), \quad (7)$$

where $E_C(\cdot)$, $E_G(\cdot)$, and $E_D(\cdot)$ represent the CNNs for the occupancy heightmap, fragility heightmap, and the avoidance heightmap, respectively, and \mathbf{f}_C , \mathbf{f}_G , and \mathbf{f}_D^b denote their learned feature maps.

Object Q-Predictor. We use the object geometric feature \mathbf{f}_P^b , the object property feature \mathbf{f}_V^b , the container’s features \mathbf{f}_C , \mathbf{f}_G , and \mathbf{f}_D^b to guide the prediction of the Q-value for varied object choices. The Dueling DQN is used and we predict the Q-

value by first predicting the state value \tilde{V}_{obj} and the predicted advantage value \tilde{A}_{obj}^b as shown below

$$\begin{aligned} \mathbf{x}_{obj}^b &= \text{concat}([\mathbf{f}_P^b, \mathbf{f}_V^b, \mathbf{f}_C, \mathbf{f}_G, \mathbf{f}_D^b]) \\ \tilde{V}_{obj} &= \Phi_V(\text{mean}_b(\mathbf{x}_{obj}^b)), \\ \tilde{A}_{obj}^b &= \Phi_A(\mathbf{x}_{obj}^b), \end{aligned} \quad (8)$$

, where $b \in \mathfrak{B}$ denotes a candidate object; \mathbf{x}_{obj}^b denotes its feature used to choose the next object to be packed; \tilde{V}_{obj} and \tilde{A}_{obj}^b are real values, and $\Phi_V(\cdot)$ and $\Phi_A(\cdot)$ are MLPs. We follow Eq.(3) to obtain the Q-value. Then, We determine the best object b^* by as the one with the highest Q-value.

Placement Q-Predictor. After determining the object, we now decide its placement, which involves the choice of orientation o , and horizontal placement (x, y) . The placement Q-predictor is formulated similarly. We use the features of the chosen object b^* and those of the container to guide the Q-value prediction of the placement choices. Similarly, before obtaining the Q-function as in Eq.(3), we first predict the state value \tilde{V}_{place} and the advantage value \tilde{A}_{place} , which is written as:

$$\begin{aligned} \mathbf{x}_{place} &= \text{concat}([\mathbf{f}_P^{b^*}, \mathbf{f}_V^{b^*}, \mathbf{f}_C, \mathbf{f}_G, \mathbf{f}_D^{b^*}, \mathbf{f}_O^{b^*}]) \\ \tilde{V}_{place} &= \Psi_V(\text{mean}_{o,x,y}(\mathbf{x}_{place})), \\ \tilde{A}_{place} &= \Psi_A(\mathbf{x}_{place}), \end{aligned} \quad (9)$$

where \mathbf{x}_{place} denote the concatenated feature of all placement options o, x and y under the chosen object b^* ; $\text{mean}_{o,x,y}(\cdot)$ denotes the mean pooling operation across all placement options; and $\Psi_V(\cdot)$ and $\Psi_A(\cdot)$ are MLPs. Same as above, we determine the best placement o^*, x^*, y^* as the one with the highest Q-value.

C. The OPA Reward Design and Network Training

We enhance the reward function to incorporate object properties, which are used to obtain ground-truth Q-values for training OPA-Net. In line with previous works [1], [6], [7], we also consider the packing compactness in our reward design. We further include pressure on the fragile object and avoidance of object relations, leading to a novel OPA reward.

First, we develop a compactness reward term to quantify the packing compactness. Following [1], we formulate the packing compactness as the ratio of the total volume of packed objects to the volume of the entire container. Let C denote the packing compactness, it can be written as:

$$C = \frac{\sum_i V_i}{H \cdot W \cdot L} \quad (10)$$

where i denotes the index for each packed object, V_i is the object's volume; H, W and L represent the height, width, and length of the container, respectively. The range of C is from 0 to 1, with a higher value indicating better space utilization.

Second, we formulate a fragility reward term and an avoidance reward term. The fragility term $R_{fragility}$ imposes a penalty for placing the selected object b^* on top of any fragile item during the current packing step, *i.e.*,

$$R_{fragility} = \mathbb{C}_{cover_fragile} \cdot \omega_{b^*}, \quad (11)$$

where $\mathbb{C}_{cover_fragile}$ counts the number of fragile objects squeezed by the object. This term is scaled by ω_{b^*} , the weight of the object, to amplify the penalty when the object is heavy. The ω_{b^*} is estimated by multiplying the volume of the object and the mean density of the density level to which it belongs.

The avoidance term $R_{avoidance}$ helps to penalize packing avoidance object pairs closely which is written as

$$R_{avoidance} = \begin{cases} 0 & \text{if } b^* \text{ is not close to any avoidance object,} \\ 1 & \text{otherwise,} \end{cases} \quad (12)$$

which is an indicating function that gives 0 when the object is not placed next to any of its avoidance objects and 1 otherwise. The values of $R_{fragility}$ and $R_{avoidance}$ are computed in the virtual environment, in which we obtain the precise positions of all packed objects.

The overall reward function is formulated as a weighted sum of the three terms, which is written as:

$$R_{overall} = \theta \cdot C - \lambda \cdot R_{fragility} - \beta \cdot R_{avoidance}, \quad (13)$$

where θ, λ , and β are hyperparameters to balance the terms.

We adopt an L2 loss as presented in Eq.(2) to train our OPA-Net. The Ground-Truth (GT) Q-values are obtained using Eq.(1) based on $R_{overall}$. As the object and the placement Q-predictors are trained separately, we obtain their GT Q-values correspondingly. We first obtain the GT Q-values for the Placement Q-Predictor. Then, we use the maximum Q-values of the same object across all candidate placements as supervision to train the Object Q-Predictor.

VI. SEQUENTIAL PACKING PROCEDURE

At test time, given an empty container and candidate objects, we perform sequential packing by iteratively selecting objects, determining placements, and packing them. Algorithm 1 illustrates a packing step. We obtain the container's occupancy heightmap \mathbf{H}_C and detect all candidate objects \mathfrak{B} as input. We also maintain a packing history list, \mathbf{His} , which records each packed object and its location, initially empty.

The algorithm for a packing step (Lines 1-16) starts by checking if the container is full or if no candidates remain, ending the process if true. Otherwise, it establishes the fragility heightmap \mathbf{H}_G based on the packing history \mathbf{His} (Line 5), and obtains the avoidance heightmap \mathbf{H}_D^b , the point clouds \mathbf{P}^b , the candidate orientations \mathbf{O}^b , and the properties \mathbf{v}^b for each candidate object b (Lines 7-8). Features are extracted using the encoders (Line 9). The Object Q-Predictor selects the optimal object b^* (Line 11), and the Placement Q-Predictor determines its placement (o^*, x^*, y^*, z^*) (Line 12). The placement is recorded, and the packing history is updated (Lines 13-14).

For object selection (Lines 17-27), we use the Object Q-Predictor to find the object with the highest Q-value. For placement selection (Lines 28-40), we first find potentially

¹We use the method proposed in [1] to efficiently find compact and placement locations by forming the object's valid placement region and then locating the convex vertices of the region as compact placement locations.

²As presented in [8]–[11], the deepest reachable z can be computed by subtracting the top-down heightmap of the container with the bottom-up heightmap of the object.

Algorithm 1 A Packing Step in Test

```

1: function PACKINGSTEP( $\mathbf{H}_C, \mathcal{B}, \mathbf{His}$ )
2:   if  $\mathcal{B} = \emptyset$  or  $Is\_Full(\mathbf{H}_C)$  then
3:     return ( $\cdot$ ),  $\mathbf{His}$ 
4:   end if
5:    $\mathbf{H}_G \leftarrow Get\_Fragile\_Map(\mathbf{His})$ 
6:   for  $b \in \mathcal{B}$  do
7:      $\mathbf{H}_D^b \leftarrow Get\_Avoidance\_Map(\mathbf{His}, b)$ 
8:      $\mathbf{P}^b, \mathbf{O}^b, \mathbf{v}^b \leftarrow Get\_Object\_Info(b)$ 
9:      $\mathbf{f}_P^b, \mathbf{f}_O^b, \mathbf{f}_V^b, \mathbf{f}_C, \mathbf{f}_G, \mathbf{f}_D^b \leftarrow Encode(\mathbf{P}^b, \mathbf{O}^b, \mathbf{v}^b,$ 
       $\mathbf{H}_C, \mathbf{H}_G, \mathbf{H}_D^b)$ 
10:   end for
11:    $b^* \leftarrow CHOOSEOBJECT(\mathcal{B}, \mathbf{f}_P^b, \mathbf{f}_V^b, \mathbf{f}_C, \mathbf{f}_G, \mathbf{f}_D^b)$ 
12:    $o^*, x^*, y^*, z^* \leftarrow CHOOSEPLACEMENT(\mathbf{O}^{b^*}, \mathbf{f}_P^{b^*}, \mathbf{f}_O^{b^*}, \mathbf{f}_V^{b^*},$ 
       $\mathbf{f}_C, \mathbf{f}_G, \mathbf{f}_D^{b^*})$ 
13:    $\mathcal{T}_{place} \leftarrow (b^*, o^*, x^*, y^*, z^*)$ 
14:    $\mathbf{His} \leftarrow [\mathbf{His}; \mathcal{T}_{place}]$ 
15:   return  $\mathcal{T}_{place}, \mathbf{His}$ 
16: end function
17: function CHOOSEOBJECT( $\mathcal{B}, \mathbf{f}_P^b, \mathbf{f}_V^b, \mathbf{f}_C, \mathbf{f}_G, \mathbf{f}_D^b$ )
18:    $Q_{obj}^* \leftarrow -\infty$ 
19:   for  $b \in \mathcal{B}$  do
20:      $Q_{obj}^b \leftarrow Object\_Q(\mathbf{f}_P^b, \mathbf{f}_V^b, \mathbf{f}_C, \mathbf{f}_G, \mathbf{f}_D^b)$ 
21:     if  $Q_{obj}^b > Q_{obj}^*$  then
22:        $Q_{obj}^* \leftarrow Q_{obj}^b$ 
23:        $b^* \leftarrow b$ 
24:     end if
25:   end for
26:   return  $b^*$ 
27: end function
28: function CHOOSEPLACEMENT( $b^*, \mathbf{H}_C, \mathbf{f}_P^{b^*}, \mathbf{f}_O^{b^*}, \mathbf{f}_V^{b^*},$ 
       $\mathbf{f}_C, \mathbf{f}_G, \mathbf{f}_D^{b^*}$ )
29:    $Q_{place}^* \leftarrow -\infty$ 
30:    $\{o, x, y\} \leftarrow Get\_All\_Placements(\mathbf{H}_C, b^*)$ 
31:   for all  $o, x, y$  do
32:      $Q_{place}^{o,x,y} \leftarrow Placement\_Q(\mathbf{f}_P^{b^*}, \mathbf{f}_O^{b^*}, \mathbf{f}_V^{b^*}, \mathbf{f}_C, \mathbf{f}_G, \mathbf{f}_D^{b^*})$ 
33:     if  $Q_{place}^{o,x,y} > Q_{place}^*$  then
34:        $Q_{place}^* \leftarrow Q_{place}^{o,x,y}$ 
35:        $o^*, x^*, y^* \leftarrow o, x, y$ 
36:     end if
37:   end for
38:    $z^* \leftarrow Get\_Depth(\mathbf{H}_C, b, o^*, x^*, y^*)$ 
39:   return  $o^*, x^*, y^*, z^*$ 
40: end function

```

compact candidate placements using [1], including possible orientations o (mainly horizontal rotations) and horizontal locations x, y . Then, we select the optimal orientation o^* and location x^*, y^* with the highest Q-value (Lines 31-37). The placement depth z^* is determined by the deepest reachable location as mentioned in [8] (Line 38).

VII. EXPERIMENTS

A. Implementation Details

Datasets. We perform experiments on the OPA dataset which includes three subsets: the Kitchen (497 objects), the Hardware

and Stationery (302 objects), and the Daily Necessities (233 objects). For more details about the dataset construction, please refer to Section IV. We train and evaluate different methods on the three subsets, presenting the individual and the overall results.

Physical simulation. We perform the virtual packing experiments on the PyBullet physical simulator. A top-down depth camera is set to capture the container’s heightmap. We follow the existing works [1], [8] to use a $32cm \times 32cm \times 30cm$ container, and all heightmaps are discretized by $1cm$ in the x and the y dimensions. We set $|\mathcal{B}| = 10$ as in [1]. For each candidate object, we consider the planner-stable poses for each object as the candidate poses and utilize the convex vertex extraction method from [1] to identify candidate packing locations. A maximum number of 500 candidate packing locations are used to determine the optimal placement in each packing step.

Network training. We set the discount factor $\gamma = 0.99$ in Eq.(1) for deep Q-learning and set $\theta = 10$, $\lambda = 20$ and $\beta = 0.2$ in Eq.(13) to weight each reward term. We use a batch size of 64 and a learning rate of 6×10^{-5} . The training process is performed on an NVIDIA GeForce RTX 2080 GPU for 24 hours, with a maximum of 3.2 million iterations.

Evaluation metrics. We evaluate the packing performance of different methods using the following metrics: (i) **Compactness**, defined as the ratio of the total volume of packed objects to the volume of the container (see Eq.(10)); (ii) **Avoidance Accuracy (Avoid. Acc.)**, i.e., the ratio packing cases without any closely-packed avoidance object pairs to the total number of packing cases; (iii) **Pressure on fragile objects (Press. on Frag.)**, defined as the mean value of the total weight applied on each fragile object by the objects placed above it. For the first two metrics, a higher value is better, while a lower value is preferred for the last metric.

B. Comparison with Existing Methods

We evaluate our method on 200 random packing sequences and compare our method with five existing packing methods: First-fit (FIRSTFIT), which is to place the object at the first feasible placement; Deepest Bottom-Left (DBL) [13], which is to find the deepest, bottom-most and left-most position for each object; Min-Z (MINZ), which is to place the object to the deepest feasible location; Heightmap-Minimization (HM) [8], [11], which is to find the object placement with minimal heightmap increment; and our baseline, the IR-BPP [1] which is a reinforcement-learning-based packing method to optimize packing compactness.

The results are shown in Table II. On average, our method achieves higher packing compactness as the baseline IR-BPP (IR-BPP 0.413 v.s. ours 0.420), while greatly improving the avoidance accuracy (Avoid. Acc.) by 42.7% and reducing the pressure on fragile objects (Press. on Frag.) by 29.4%. It consistently outperforms IR-BPP in the two metrics across the three subsets. Compared with FIRSTFIT, DBL, HM and MINZ, our method significantly enhances the packing compactness by at least 42.9% and improves the avoidance

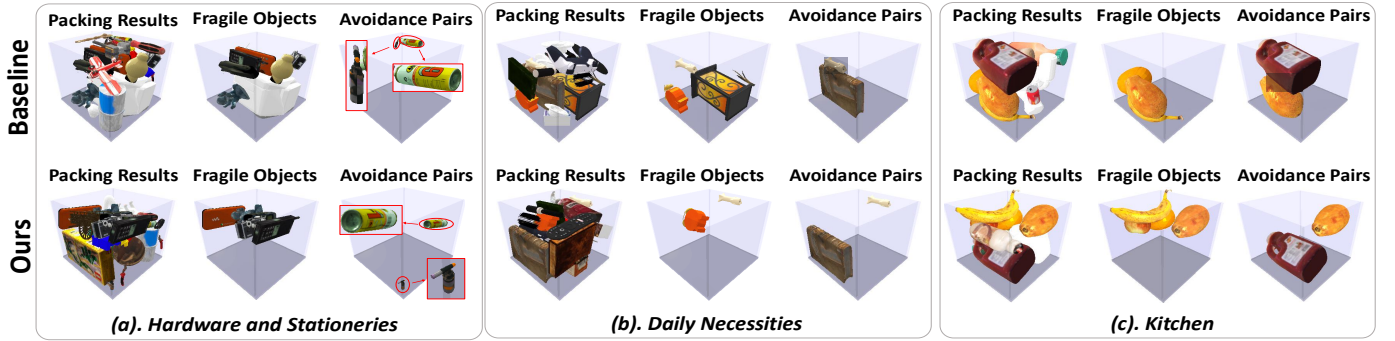


Fig. 5. Visualization of the packing results produced by the baseline [1] and our method from each of the following subsets: Hardware and Stationeries, Daily Necessities, and Kitchen. In each case, we first display the overall packing results in the first column, followed by a visualization of the fragile objects in the second column, and finally an avoidance object pair in the last column. Compared to the baseline, our method tends to position fragile objects on top to prevent compression from heavier items and more effectively separates avoidance object pairs.

TABLE II

COMPARING THE AVERAGE PERFORMANCE OF DIFFERENT PACKING METHODS OVER 200 RANDOM SEQUENCES. OUR METHOD CAN MAINTAIN HIGH PACKING COMPACTNESS WHILE SEPARATING AVOIDANCE PAIRS AND GREATLY REDUCE THE PRESSURE ON FRAGILE OBJECTS.

Average			
Method	Compactness \uparrow	Avoid. Acc. \uparrow	Press. on Frag. \downarrow
FIRSTFIT	0.243	76.33%	3.10
DBL	0.288	78.83%	5.00
HM	0.278	81.17%	4.86
MINZ	0.289	78.83%	4.93
IR-BPP (Baseline)	0.420	52.33%	5.07
Ours	0.413	95.00%	3.58
Hardware & Stationery			
Method	Compactness \uparrow	Avoid. Acc. \uparrow	Press. on Frag. \downarrow
FIRSTFIT	0.234	82.5%	3.92
DBL	0.270	81.0%	6.82
HM	0.263	86.0%	6.29
MINZ	0.274	86.0%	7.13
IR-BPP (Baseline)	0.400	64.5%	6.55
Ours	0.392	94.0%	3.76
Daily Necessities			
Method	Compactness \uparrow	Avoid. Acc. \uparrow	Press. on Frag. \downarrow
FIRSTFIT	0.226	77.5%	2.47
DBL	0.256	85.5%	3.43
HM	0.242	87.0%	3.54
MINZ	0.258	79.0%	3.37
IR-BPP (Baseline)	0.418	52.5%	4.30
Ours	0.415	94.0%	3.52
Kitchen			
Method	Compactness \uparrow	Avoid. Acc. \uparrow	Press. on Frag. \downarrow
FIRSTFIT	0.268	69.0%	2.91
DBL	0.338	70.0%	4.76
HM	0.329	70.5%	4.75
MINZ	0.335	71.5%	4.31
IR-BPP (Baseline)	0.443	40.0%	4.36
Ours	0.434	97.0%	3.45

accuracy by at least 13.8% with slight pressure on fragile objects.

In addition, we visually compare the packing results produced by our method and those produced by IR-BPP, and the results are shown in Figure 5. We visualize the results from the three subsets respectively, and the comparisons are made in the same packing cases. The results indicate that our method has a trend of placing fragile objects on top of the pile to reduce their pressure. In contrast, the baseline fails to achieve

this goal due to its lack of awareness of object’s fragility. Moreover, our method more effectively avoids closely-packed unsuitable object pairs compared to the baseline. Again, this is because our method is aware of the object’s avoidance relations when learning the packing strategies. With these features, our method helps to enhance overall safety and intelligence in packing planning.

C. Object Property Recognition Results

Our object property recognition scheme achieves a high accuracy of over 90%. More statistical results together with the ablation studies are shown in Section VII-D. In this section, we show some property recognition results produced by our method in Figure 6. We visualize four objects from each subset of our OPA dataset. The object class names are provided as input, and we first infer the object’s inner and outer materials for the chain-of-thought reasoning. We predict single-material objects, like the ceramic mug and organic fig. For multi-material items, we identify both the inner and outer materials. For example, the drill and screwdriver are plastic outside and metal inside; the vial is glass externally and liquid internally; and the cigarettes are cardboard outside and tobacco inside.

Then, our method recognizes each object’s physical properties (i.e., fragility, softness, sharpness and density level). It identifies the vial, mug, candle, and fig as fragile objects; the soccer ball, candle, and fig as soft objects; the drill, hammer, screwdriver, and knife as sharp objects. It also accurately predicts the density level for each object. For example, high-density items, like the drill and knife, have a density level of five; medium-density objects, such as detergent and the vial, are rated at three; and light items, like the soccer ball and cigarettes, have a density level of one.

Furthermore, our method identifies semantic properties, recognizing the fig as an edible item, the detergent as a household chemical, the vial as medicine, and the candle, the cigarettes as ignition sources, and identifying the vial, the candle, and the cigarettes as flammable items.

D. Ablation Studies

We perform ablation studies to evaluate the effectiveness of each design. Specifically, we individually remove each



Fig. 6. Visualization of the property recognition results in our OPA dataset. Our method provides detailed object property annotations, correctly predicting physical attributes like fragility, softness, and weight density, as well as semantic properties such as edibility, household chemicals, medicine, ignition items, and flammable items. Best viewed in color.

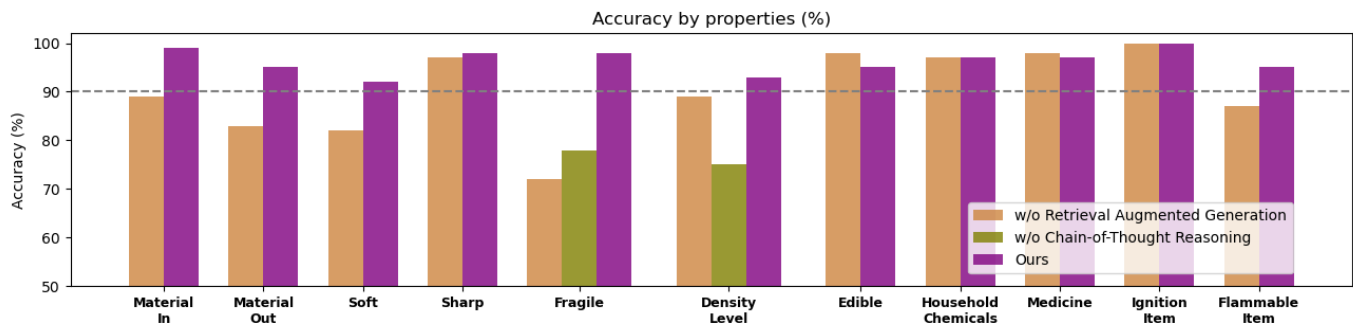


Fig. 7. The ablation studies on each design of our object property recognition scheme. The annotation accuracies are obtained on 100 randomly selected objects from the OPA dataset. The use of retrieval augmented generation and chain-of-thought reasoning helps our method to achieve accurate object property recognition. Best viewed in color.

component in the object property recognition and the object-property-aware packing learning.

Object Property Recognition. We evaluate the effectiveness of the following two designs in our object property recognition: (i) the retrieval augmented generation, i.e., using a small human annotated subset to guide the prediction; (ii) the chain-of-thought reasoning, i.e., predicting the object’s inner and outer materials first before obtaining the fragility and the density level. To assess the annotation quality of different designs, we randomly selected 100 objects from the OPA dataset and asked a human participant to evaluate the accuracy

of the VLM’s property recognition.

The results are shown in Figure 7. First, we remove the retrieval augmented generation, allowing the VLM to predict object properties directly without the guidance of the annotated subset. In most properties, the results of “w/o Retrieval Augmented Generation” show a noticeable performance drop consistently in each object property compared with the full recognition scheme “Ours”. This evidences the significance of retrieval augmented generation in achieving accurate property recognition. Second, we eliminate the chain-of-thought reasoning (indicated as “w/o Chain-of-Thought Reasoning”), which means we directly predict fragility and density levels.

TABLE III
 ABLATION STUDIES OF OUR NETWORK DESIGN. ALL THE FRAGILITY REWARD TERM, THE AVOIDANCE REWARD TERM, AND THE NETWORK ARCHITECTURE CONTRIBUTE TO IMPROVING THE PACKING COMPACTNESS, INCREASING THE AVOIDANCE ACCURACY, AND REDUCING THE PRESSURE ON FRAGILE OBJECTS.

	$R_{fragility}$	$R_{avoidance}$	Property-Embedding	Map Encoders	Compactness \uparrow	Avoid. Acc. \uparrow	Press. on Frag. \downarrow
Average					0.420	52.33%	5.07
	✓				0.419	83.33%	4.45
	✓	✓			0.378	91.50%	4.23
	✓	✓	✓		0.412	92.50%	3.86
	✓	✓	✓	✓	0.413	95.00%	3.58
Hardware & Stationery					0.400	64.50%	6.55
	✓				0.384	82.00%	4.73
	✓	✓			0.371	89.50%	4.68
	✓	✓	✓		0.391	91.50%	4.26
	✓	✓	✓	✓	0.392	94.00%	3.76
Daily Necessities					0.418	52.50%	4.30
	✓				0.439	86.50%	4.89
	✓	✓			0.408	91.00%	4.24
	✓	✓	✓		0.406	94.00%	3.76
	✓	✓	✓	✓	0.415	94.00%	3.52
Kitchen					0.443	40.00%	4.36
	✓				0.435	81.50%	3.72
	✓	✓			0.372	94.00%	3.40
	✓	✓	✓		0.440	92.00%	3.56
	✓	✓	✓	✓	0.434	97.00%	3.45

This approach bypasses the initial step of predicting the inner and outer materials first before deriving the fragility and density levels. Removing chain-of-thought reasoning results in a noticeable performance drop of over 10% in the annotation of both fragility and density levels, which shows the necessity of using chain-of-thought reasoning in our object property annotation scheme.

Object-Property-Aware Packing. Additionally, we conduct ablation studies on each component of our object-property-aware packing learning, and the results are shown in Table III. We start from the baseline which only contains components required to optimize packing compactness, i.e., the object geometric encoder $E_P(\cdot)$, the candidate pose-embedding layer $E_O(\cdot)$, the container’s occupancy heightmap \mathbf{H}_C , the Object Q-Predictor, the Placement Q-Predictor and the compactness reward of Eq.(10). Then, we gradually include the fragility reward term $R_{fragility}$ and the avoidance reward term $R_{avoidance}$ from the baseline to avoid closely packed inappropriate object pairs and reduce the pressure on fragile objects. In addition, we include the use of the property-embedding layer $E_V(\cdot)$ (shown as “Property-Embedding” in Table III) to encode the property for each candidate object to optimize the packing objectives better. Finally, we further integrate the design of encoding the fragility heightmap \mathbf{H}_G and avoidance heightmap \mathbf{H}_D (shown as “Map Encoders” in Table III) to indicate the locations of the previously packed fragile and avoidance objects for the property-aware learning.

From the results, we can see that incorporating the fragility reward term reduces pressure on fragile objects, with an average decrease of 12%. Moreover, by further incorporating the avoidance reward term, we not only reduce the pressure on fragile objects but also significantly improve the avoidance accuracy by 39.17% compared to the baseline that lacks both reward terms. These results demonstrate the effectiveness of the reward design. However, only including the reward terms

TABLE IV
 PARAMETER ANALYSIS ON THE OPA DATASET. WE PRESENT THE AVERAGED RESULTS ACROSS THE THREE SUBSETS. IN ORDER TO BALANCE THE THREE METRICS, WE CHOOSE $\lambda = 20$ AND $\beta = 0.2$ IN OUR MAIN EXPERIMENT.

OPA dataset			
	Press. on Frag. \downarrow	Compactness \uparrow	Avoid. Acc. \uparrow
$\lambda = 2$	4.38	0.423	91.00%
$\lambda = 20$	3.58	0.413	95.00%
$\lambda = 200$	3.51	0.344	92.33%
OPA dataset			
	Avoid. Acc. \uparrow	Compactness \uparrow	Press. on Frag. \downarrow
$\beta = 0.02$	76.33%	0.424	3.32
$\beta = 0.2$	95.00%	0.413	3.58
$\beta = 2$	96.50%	0.378	3.29

$R_{fragility}$ and $R_{avoidance}$ has sub-optimal packing compactness because the network does not separately encode object properties and geometries, making it challenging to balance packing compactness with property-related packing objectives. After including the property-embedding layer, the fragility heightmap, and the avoidance heightmap, the performance enhanced consistently in the three metrics, achieving an increase of 3.5% in packing compactness, an improvement of 4% in avoidance accuracy and a reduction of 15% in pressure on fragile objects. These results demonstrate the necessity of our reward design and the network architecture design.

E. Parameter Analysis

In addition, we perform a parameter analysis on λ and β in the reward design (see Eq.(1)), evaluating the performance of our method with adjusted parameters. Here, λ represents the weight of the fragility reward term, while β denotes the weight of the avoidance term. A higher λ imposes a stronger penalty for packing items on top of a fragile object, whereas a higher β enforces a stronger penalty for placing avoidance object pairs too closely. Specifically, we scale down and scale

TABLE V

COMPARING THE AVERAGE PERFORMANCE OF OUR METHOD AND THE BASELINE OVER 200 RANDOM SEQUENCES ON THE REAL OBJECTS IN THE PHYSICAL SIMULATOR. COMPARED WITH THE BASELINE, OUR METHOD ACHIEVES HIGHER AVOIDANCE ACCURACY AND REDUCES THE PRESSURE ON FRAGILE OBJECTS WHILE MAINTAINING SIMILAR COMPACTNESS.

Real-scanned Objects			
Method	Compactness \uparrow	Avoid. Acc. \uparrow	Press. on Frag. \downarrow
DBL	0.441	83.0%	1.75
HM	0.430	86.0%	1.51
MINZ	0.446	87.5%	1.63
IR-BPP (Baseline)	0.606	71.0%	1.16
Ours	0.585	94.5%	0.90

up β and λ by 10 times separately, and present the results of the related metrics. The results are shown in Table IV.

The results indicate that decreasing λ to 2 leads to a noticeable increase of 22% in pressure on fragile objects. While compared with $\lambda = 20$, increasing λ to 200 can reduce the pressure on fragile objects by 2%, it substantially hampers packing compactness by 6.9% due to an imbalance among the reward terms. Consequently, we opt for $\lambda = 20$ in our implementation, as this maintains good packing compactness while achieving a relatively low pressure on fragile objects. Similarly, when scaling down β to 0.02, a great drop of 18.67% is observed in the avoidance accuracy. Although scaling up β to 2 results in a slight increase of 1.5% in the avoidance accuracy, the packing compactness drops by 3.5%. Therefore, we set $\beta = 0.2$ in our implementation.

F. Extension to Real-scanned Objects

In addition to the objects in the OPA dataset, we also collect a dataset comprising 87 real-scanned items from supermarkets and evaluate our method on these items. Specifically, we scan the CAD model of each object using the Scan3D App, and then perform the object property recognition as presented in Section IV. We load the objects in the virtual environment for the packing training and compare the performance of our method and IR-BPP (our baseline) [1]. The results are shown in Table V.

From the results, we can see that our method can still maintain similar packing compactness as the baseline on the real-scanned objects. In addition, it achieves a high avoidance accuracy of 94.5%, surpassing the baseline by 23.5%. At the same time, it greatly reduces the pressure on fragile objects by 22.4% compared with the baseline. These results have demonstrated the effectiveness of our OPA-Pack in real-scanned objects.

VIII. ROBOTIC PACKING ON PHYSICAL PLATFORM

A. Platform Setup

Hardware. Our real-world robotic packing system involves the NACHI MZ07 Robot with a suction cup to manipulate the objects, and a Photoneo camera to capture the top-down point clouds of the container and the buffer area. A buffer area consists of 5 regions, each of which holds an object. The buffer area is manually filled when all objects are packed by the robot. We use a container with a size of $30\text{cm} \times 30\text{cm} \times 20\text{cm}$

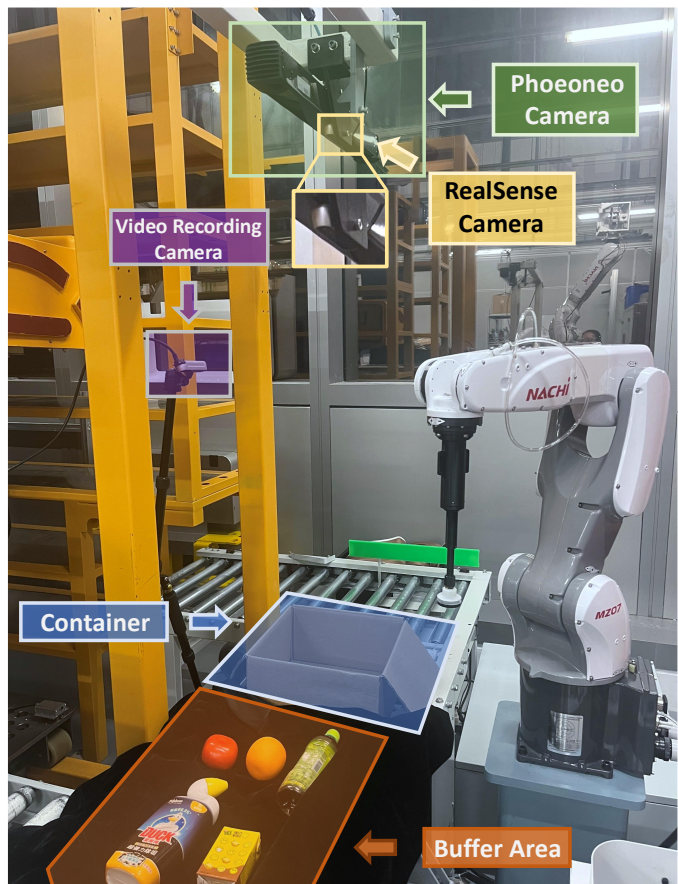


Fig. 8. Our physical packing platform with a NACHI MZ07 robot arm. A buffer area (orange, bottom) is set to store five candidate objects; a container (blue, medium) is used for packing objects; a Photoneo camera (green, top) is set for depth sensing; a RealSense (yellow, top) camera is used to capture the RGB image; and another camera (purple, top-left) is mounted on a tripod for video recording. Best viewed in color.

for packing the objects. Our packing platform setup is shown in Figure 8.

Packing Pipeline. Executing a real-world packing sequence involves multiple packing steps of selecting and loading an object into the container. In our platform, a packing step involves four stages: (1) identifying the objects in the buffer area and selecting the candidate object, (2) estimating its initial pose, (3) determining its placement pose inside the container, (4) generating and executing the robotic pick-and-place action. It also involves basic error recovery designs, such as picking failure detection and sensing errors. In the following, we introduce the details for object identification and selection, object pose estimation, placement determination, pick-and-place action generation, and error recovery designs in our physical platform.

Object Identification and Selection. We identify objects in the buffer area based on the scanned point cloud. For each region of the buffer area, we create a bounding box slightly above the plane, and crop local point clouds. If the number of points in the bounding box reaches 150, the region is considered non-empty.

We perform a CLIP-based [42] object retrieval to identify



Fig. 9. Visual comparison of our method and the baseline in real-world packing results. Left: our method better prevents heavy objects from being placed on fragile persimmon, addressing a limitation of the baseline. By employing our approach, we can reduce fruit damage. Right: the baseline packs the persimmon directly on top of the medical kit, which could contaminate the unsealed fresh fruit. In comparison, our method avoids packing them closely.

the object. Specifically, we maintain a database that contains RGB patch templates for each object type. Each object type may have multiple templates showcasing different views (e.g., the front view and the back view) and variations of the objects (e.g., the same sugar type of different flavors). To accommodate different object sizes, we zero-pad the patch templates to 360×360 pixels. Next, we extract the CLIP feature for each patch template in the database to serve as references. For each non-empty region in the buffer area, we perform the same preprocessing and compare its CLIP features to that of the templates using the cosine distance. The template with the closest distance is retrieved as the best match, allowing us to identify the corresponding object type. This process is repeated for each object in the buffer area until all objects are recognized.

Finally, we retrieve the CAD models for all detected object types into the Object Q-Predictor to select the object for packing. The model predicts the Q-values for each object type, and the one with the highest Q-value is determined as the next object to be packed.

Pose Estimation. Once the Object Q-Predictor selects the object, we crop its real-scanned point cloud and conduct pose estimation to obtain the object’s initial orientation for more accurate packing planning. The object point clouds are downsampled to a voxel size of 1mm and denoised to remove statistical outliers. We also load the virtual CAD model of the object and sample a virtual point cloud. Next, we extract Fast Point Feature Histograms (FPFH) descriptors from both the virtual and real-scanned point clouds to identify matched point pairs. For each virtual and real object pair, we apply a RANSAC-based feature-matching algorithm to obtain a coarse pose estimation, followed by the Iterative Closest Point (ICP) algorithm to refine the pose estimation.

Placement Determination. After performing object pose estimation, we obtain a precise pose for the chosen object, reorient its CAD model, and feed it to the Placement Q-Predictor to determine the placement pose. When considering different

placement poses, we account for in-plane rotations along the z-axis and model 8 orientations for each object. The placement pose is defined by the object’s geometric center after it is placed inside the container.

Pick-and-place Action Generation. Using the estimated initial pose of the selected object, we first identify the coarse horizontal picking locations of the object based on the geometric center of the rotated CAD model. Next, we project the horizontal locations onto the real-scanned point cloud to retrieve a set of surface points. We then compute the curvature of each point and select the one with the lowest curvature as the picking center, which helps us determine the exact picking location (x, y, z). The approaching direction for picking is defined by the surface normal at the picking center. The placement action uses a vertical placement direction at the target placement center.

Error Recovery. The system features an error recovery mechanism that includes re-scanning and re-picking schemes. After scanning the packing scene, it checks if the number of points in the whole-scene point clouds meets the number of points in a normal scan. If it falls below 80% of this threshold, the camera re-scans the scene. This process is crucial since the camera sensing operates in a parallel thread alongside the robot arm, with communication handled via signals. If a signal disruption leads to an early or late sensing while the robot arm is in the working area (i.e., the buffer area and the container), a large region would be missing from the resulting point cloud due to the robot arm’s reflection. The re-scanning scheme helps avoid erroneous robotic actions that could damage nearby facilities. The system also detects picking failures by continuously monitoring the atmospheric pressure in the suction cup. If low pressure is detected after an attempted pick, it indicates that the object was not successfully lifted. In this case, the system stops the current packing step, allows the robot arm to retract from the working area, and re-scan the buffer area to perform again the pick attempt.

TABLE VI

COMPARING THE AVERAGE PERFORMANCE OF OUR METHOD AND THE BASELINE OVER 50 REAL-WORLD PACKING CASES. OUR METHOD ACHIEVES SIMILAR PACKING COMPACTNESS AS THE BASELINE WHILE REDUCING THE NUMBER OF CLOSELY PACKED AVOIDANCE OBJECT PAIRS AND THE NUMBER OF SQUEEZED FRAGILE OBJECTS.

Method	Compactness \uparrow	# Close Avoid. Pairs \downarrow	# Squeeze Fragile \downarrow
DBL	0.28	1.50	0.80
HM	0.30	1.01	0.86
MINZ	0.27	1.37	0.70
IR-BPP (Baseline)	0.34	0.94	0.74
Ours	0.33	0.54	0.14

B. Real-world Packing Results

We perform real-world packing experiments on 50 random packing sequences, each containing 10 random objects. We compare our model with three packing heuristics: (1) the Deepest Bottom-Left (DBL) [13], (2) the Min-Z (MINZ), (3) the Heightmap-Minimization (HM) [8], [11], as well as our baseline method, the IR-BPP [1] which is based on reinforcement learning. All comparisons are made under the same packing sequences. Three evaluation metrics are used to evaluate the packing performance: (1) the compactness, which is the ratio of the total volume of all packed objects and the total volume of the container; (2) the number of closely packed avoidance pairs (# Close Avoid. Pair) and (3) the number of fragile objects compressed by heavy objects (# Squeeze Fragile) in each sequence. The compactness is higher the better, while the other two metrics are lower the better. The average results across all sequences are shown in Table VI.

The results indicate that our method achieves a high packing compactness similar to the baseline, IR-BPP, out-performing all packing heuristics. At the same time, compared with the IR-BPP, we significantly reduce the number of closely packed avoidance pairs by over 42.6% and decrease the number of squeezed fragile objects by over 5 times. We also provide a visualization of two real-world example cases produced by the baseline and our method in Figure 9. The results in Figure 9 (left) indicate that the baseline can crush fragile fruits, *i.e.*, the persimmon, by unconsciously packing heavy drinks on top of them, while our method can better protect the fragile objects by preventing such placements. The results in Figure 9 (right) show that our method can avoid packing the medical test kit with the persimmon closely while the baseline fails to do so. These findings further demonstrate the effectiveness of our OPA-Pack in real-world packing scenarios, maintaining compactness while minimizing the squeezing of fragile objects and separating avoidance pairs. Please refer to our supplemental materials for more results.

CONCLUSION

This paper introduces OPA-Pack, the first robotic bin packing framework incorporating object that considers object properties. We develop an object property recognition scheme with retrieval augmented generation and chain-of-thought reasoning to predict object-centric properties. The object-centric properties are then used to derive property-based avoidance relations between object pairs. A dataset of 1,032 everyday

objects with property annotations is established for object-property-aware packing learning. In addition, we formulate OPA-Net, aiming to reduce the pressure on fragile object and avoid packing incompatible object pairs closely, while maintaining a compact bin packing. Extensive experiments conducted in both a virtual simulator and a real-world platform demonstrate the effectiveness of our method. Our method can significantly improve the avoidance accuracy by 42.7% and reduce the pressure on fragile objects by 29.4% in the physical simulator, while achieving comparable packing compactness. Moreover, it reduces the number of closely packed avoidance pairs by 42.5% and decreases the number of squeezed fragile objects by over 5 times in the real-world platform.

Nonetheless, this work has certain limitations that can be addressed in future research. First, our method mainly optimizes for predefined packing preferences, *i.e.*, reduction of pressure on fragile objects and avoidance of closely packed incompatible object pairs. It has not considered a test-time modification of the user’s packing preference. An interesting future direction is to enable on-the-fly change of the packing preferences. Second, it focuses mainly on packing objects to a single container. In the future, we can plan to extend our method to multi-container packing scenarios, using the Hungarian algorithm to distribute objects into different containers, preventing fragile objects from being squeezed and avoiding closely packed avoidance object pairs. Third, although our method selects from compact and stable placement candidates, objects may still shift after placement. We will incorporate object tracking to better monitor the locations of packed objects in future developments.

REFERENCES

- [1] H. Zhao, Z. Pan, Y. Yu, and K. Xu, “Learning physically realizable skills for online packing of general 3D shapes,” *ACM Transactions on Graphics*, vol. 42, no. 5, pp. 1–21, 2023.
- [2] Y. Ma, Z. Chen, W. Hu, and W. Wang, “Packing irregular objects in 3D space via hybrid optimization,” in *Computer Graphics Forum*, vol. 37, no. 5. Wiley Online Library, 2018, pp. 49–59.
- [3] S. Yang, S. Song, S. Chu, R. Song, J. Cheng, Y. Li, and W. Zhang, “Heuristics integrated deep reinforcement learning for online 3D bin packing,” *IEEE Transactions on Automation Science and Engineering*, 2023.
- [4] J. Jia, H. Shang, and X. Chen, “Robot online 3D bin packing strategy based on deep reinforcement learning and 3D vision,” in *IEEE International Conference on Networking, Sensing and Control*. IEEE, 2022, pp. 1–6.
- [5] A. V. Puche and S. Lee, “Online 3D bin packing reinforcement learning solution with buffer,” in *IEEE/RSJ International Conference on Intelligent Robots and Systems*. IEEE, 2022, pp. 8902–8909.
- [6] S. Huang, Z. Wang, J. Zhou, and J. Lu, “Planning irregular object packing via hierarchical reinforcement learning,” *IEEE Robotics and Automation Letters*, vol. 8, no. 1, pp. 81–88, 2022.
- [7] R. Hu, J. Xu, B. Chen, M. Gong, H. Zhang, and H. Huang, “TAP-Net: transport-and-pack using reinforcement learning,” *ACM Transactions on Graphics*, vol. 39, no. 6, pp. 1–15, 2020.
- [8] F. Wang and K. Hauser, “Stable bin packing of non-convex 3D objects with a robot manipulator,” in *2019 International Conference on Robotics and Automation*. IEEE, 2019, pp. 8698–8704.
- [9] J.-H. Pan, K.-H. Hui, X. Gao, S. Zhu, Y.-H. Liu, P.-A. Heng, and C.-W. Fu, “Sdf-pack: Towards compact bin packing with signed-distance-field minimization,” in *2023 IEEE/RSJ International Conference on Intelligent Robots and Systems (IROS)*. IEEE, 2023, pp. 10 612–10 619.
- [10] J.-H. Pan, X. Gao, K.-H. Hui, S. Zhu, Y.-H. Liu, P.-A. Heng, and C.-W. Fu, “PPN-Pack: Placement proposal network for efficient robotic bin packing,” *IEEE Robotics and Automation Letters*, 2024.

- [11] F. Wang and K. Hauser, "Dense robotic packing of irregular and novel 3d objects," *IEEE Transactions on Robotics*, vol. 38, no. 2, pp. 1160–1173, 2021.
- [12] A. G. Ramos, J. F. Oliveira, J. F. Gonçalves, and M. P. Lopes, "A container loading algorithm with static mechanical equilibrium stability constraints," *Transportation Research Part B: Methodological*, vol. 91, pp. 565–581, 2016.
- [13] K. Karabulut and M. M. İnceoğlu, "A hybrid genetic algorithm for packing in 3D with deepest bottom left with fill method," in *International Conference on Advances in Information Systems*. Springer, 2004, pp. 441–450.
- [14] K. Kang, I. Moon, and H. Wang, "A hybrid genetic algorithm with a new packing strategy for the three-dimensional bin packing problem," *Applied Mathematics and Computation*, vol. 219, no. 3, pp. 1287–1299, 2012.
- [15] T. G. Crainic, G. Perboli, and R. Tadei, "Extreme point-based heuristics for three-dimensional bin packing," *Informatics Journal on computing*, vol. 20, no. 3, pp. 368–384, 2008.
- [16] X. Liu, J.-M. Liu, A.-X. Cao, and Z.-L. Yao, "HAPE3D—a new constructive algorithm for the 3D irregular packing problem," *Frontiers of Information Technology & Electronic Engineering*, vol. 16, no. 5, pp. 380–390, 2015.
- [17] C. Lamas-Fernandez, J. A. Bennell, and A. Martinez-Sykora, "Voxel-based solution approaches to the three-dimensional irregular packing problem," *Operations Research*, 2022.
- [18] Y. Jiang, M. Lim, C. Zheng, and A. Saxena, "Learning to place new objects in a scene," *The International Journal of Robotics Research*, vol. 31, no. 9, pp. 1021–1043, 2012.
- [19] H. Zhao, Q. She, C. Zhu, Y. Yang, and K. Xu, "Online 3D bin packing with constrained deep reinforcement learning," in *Proceedings of the AAAI Conference on Artificial Intelligence*, vol. 35, no. 1, 2021, pp. 741–749.
- [20] R. Verma, A. Singhal, H. Khadilkar, A. Basumatary, S. Nayak, H. V. Singh, S. Kumar, and R. Sinha, "A generalized reinforcement learning algorithm for online 3d bin-packing," *arXiv preprint arXiv:2007.00463*, 2020.
- [21] J. Zhang, B. Zi, and X. Ge, "Attend2Pack: Bin packing through deep reinforcement learning with attention," in *2021 International Conference on Machine Learning Workshops*, 2021.
- [22] Y. Pan, Y. Chen, and F. Lin, "Adjustable robust reinforcement learning for online 3d bin packing," *Advances in Neural Information Processing Systems*, vol. 36, pp. 51 926–51 954, 2023.
- [23] Z. Yang, S. Yang, S. Song, W. Zhang, R. Song, J. Cheng, and Y. Li, "PackerBot: Variable-sized product packing with heuristic deep reinforcement learning," in *IEEE/RSJ International Conference on Intelligent Robots and Systems*. IEEE, 2021, pp. 5002–5008.
- [24] I. Moon and T. V. L. Nguyen, "Container packing problem with balance constraints," *OR spectrum*, vol. 36, no. 4, pp. 837–878, 2014.
- [25] T. A. de Queiroz and F. K. Miyazawa, "Two-dimensional strip packing problem with load balancing, load bearing and multi-drop constraints," *International Journal of Production Economics*, vol. 145, no. 2, pp. 511–530, 2013.
- [26] R. Firoozi, J. Tucker, S. Tian, A. Majumdar, J. Sun, W. Liu, Y. Zhu, S. Song, A. Kapoor, K. Hausman, *et al.*, "Foundation models in robotics: Applications, challenges, and the future," *The International Journal of Robotics Research*, p. 02783649241281508, 2023.
- [27] X. Li, M. Zhang, Y. Geng, H. Geng, Y. Long, Y. Shen, R. Zhang, J. Liu, and H. Dong, "Manipllm: Embodied multimodal large language model for object-centric robotic manipulation," in *Proceedings of the IEEE/CVF Conference on Computer Vision and Pattern Recognition*, 2024, pp. 18 061–18 070.
- [28] F. Ni, J. Hao, S. Wu, L. Kou, J. Liu, Y. Zheng, B. Wang, and Y. Zhuang, "Generate subgoal images before act: Unlocking the chain-of-thought reasoning in diffusion model for robot manipulation with multimodal prompts," in *Proceedings of the IEEE/CVF Conference on Computer Vision and Pattern Recognition*, 2024, pp. 13 991–14 000.
- [29] W. Huang, C. Wang, R. Zhang, Y. Li, J. Wu, and L. Fei-Fei, "Voxposer: Composable 3d value maps for robotic manipulation with language models," *arXiv preprint arXiv:2307.05973*, 2023.
- [30] J. Yang, Y. Dong, S. Liu, B. Li, Z. Wang, H. Tan, C. Jiang, J. Kang, Y. Zhang, K. Zhou, *et al.*, "Octopus: Embodied vision-language programmer from environmental feedback," in *European Conference on Computer Vision*. Springer, 2025, pp. 20–38.
- [31] W. Huang, C. Wang, Y. Li, R. Zhang, and L. Fei-Fei, "Rekep: Spatio-temporal reasoning of relational keypoint constraints for robotic manipulation," *arXiv preprint arXiv:2409.01652*, 2024.
- [32] N. Di Palo and E. Johns, "Keypoint action tokens enable in-context imitation learning in robotics," *arXiv preprint arXiv:2403.19578*, 2024.
- [33] R. Bommasani, D. A. Hudson, E. Adeli, R. Altman, S. Arora, S. von Arx, M. S. Bernstein, J. Bohg, A. Bosselut, E. Brunskill, *et al.*, "On the opportunities and risks of foundation models," *arXiv preprint arXiv:2108.07258*, 2021.
- [34] J. Achiam, S. Adler, S. Agarwal, L. Ahmad, I. Akkaya, F. L. Aleman, D. Almeida, J. Altenschmidt, S. Altman, S. Anadkat, *et al.*, "Gpt-4 technical report," *arXiv preprint arXiv:2303.08774*, 2023.
- [35] Z. Xu, C. Gao, Z. Liu, G. Yang, C. Tie, H. Zheng, H. Zhou, W. Peng, D. Wang, T. Chen, *et al.*, "Manifoundation model for general-purpose robotic manipulation of contact synthesis with arbitrary objects and robots," *arXiv preprint arXiv:2405.06964*, 2024.
- [36] P. Zhao, H. Zhang, Q. Yu, Z. Wang, Y. Geng, F. Fu, L. Yang, W. Zhang, and B. Cui, "Retrieval-augmented generation for ai-generated content: A survey," *arXiv preprint arXiv:2402.19473*, 2024.
- [37] P. Lewis, E. Perez, A. Piktus, F. Petroni, V. Karpukhin, N. Goyal, H. Küttler, M. Lewis, W.-t. Yih, T. Rocktäschel, *et al.*, "Retrieval-augmented generation for knowledge-intensive nlp tasks," *Advances in Neural Information Processing Systems*, vol. 33, pp. 9459–9474, 2020.
- [38] J. Wei, X. Wang, D. Schuurmans, M. Bosma, F. Xia, E. Chi, Q. V. Le, D. Zhou, *et al.*, "Chain-of-thought prompting elicits reasoning in large language models," *Advances in neural information processing systems*, vol. 35, pp. 24 824–24 837, 2022.
- [39] G. Feng, B. Zhang, Y. Gu, H. Ye, D. He, and L. Wang, "Towards revealing the mystery behind chain of thought: a theoretical perspective," *Advances in Neural Information Processing Systems*, vol. 36, 2024.
- [40] Z. Zhang, A. Zhang, M. Li, and A. Smola, "Automatic chain of thought prompting in large language models," in *The Eleventh International Conference on Learning Representations*.
- [41] Z. Chu, J. Chen, Q. Chen, W. Yu, T. He, H. Wang, W. Peng, M. Liu, B. Qin, and T. Liu, "A survey of chain of thought reasoning: Advances, frontiers and future," *arXiv preprint arXiv:2309.15402*, 2023.
- [42] A. Radford, J. W. Kim, C. Hallacy, A. Ramesh, G. Goh, S. Agarwal, G. Sastry, A. Askell, P. Mishkin, J. Clark, *et al.*, "Learning transferable visual models from natural language supervision," in *International conference on machine learning*. PMLR, 2021, pp. 8748–8763.
- [43] OpenAI, "Chatgpt-4," <https://chat.openai.com/chat>, 2023.
- [44] B. Calli, A. Walsman, A. Singh, S. Srinivasa, P. Abbeel, and A. M. Dollar, "Benchmarking in manipulation research: Using the Yale-CMU-Berkeley object and model set," *IEEE Robotics & Automation Magazine*, vol. 22, no. 3, pp. 36–52, 2015.
- [45] M. Deitke, D. Schwenk, J. Salvador, L. Weihs, O. Michel, E. VanderBilt, L. Schmidt, K. Ehsani, A. Kembhavi, and A. Farhadi, "Objaverse: A universe of annotated 3d objects," in *Proceedings of the IEEE/CVF Conference on Computer Vision and Pattern Recognition*, 2023, pp. 13 142–13 153.
- [46] H. Zhao, Y. Yu, and K. Xu, "Learning efficient online 3D bin packing on packing configuration trees," in *International Conference on Learning Representations*, 2021.
- [47] C. J. Watkins and P. Dayan, "Q-learning," *Machine learning*, vol. 8, pp. 279–292, 1992.
- [48] Z. Wang, T. Schaul, M. Hessel, H. Hasselt, M. Lanctot, and N. Freitas, "Dueling network architectures for deep reinforcement learning," in *International conference on machine learning*. PMLR, 2016, pp. 1995–2003.
- [49] C. R. Qi, H. Su, K. Mo, and L. J. Guibas, "PointNet: Deep learning on point sets for 3d classification and segmentation," in *Proceedings of the IEEE conference on computer vision and pattern recognition*, 2017, pp. 652–660.